Nonlinear Integral Formulation and Neural Network-Based Solution for Reconstruction of Deep Defects With Pulse Eddy Currents

Gabriel Preda and Florea I. Hantila

Electrical Engineering Department, Politehnica University of Bucharest, Bucharest 060042, Romania

A method for reconstruction of defects buried deep under material surface of conductive nonlinear materials is proposed. Defects are approximated as zero thickness. Simulation of pulse eddy currents is done using an integral FEM method, with a polarization method with over-relaxation to speed up the nonlinear iterations, and a neural network method is used for the reconstruction of defects shape from the simulated signals.

Index Terms— **Eddy currents, neural networks (NNs), nondestructive testing, nonlinear magnetic.**

I. Introduction

In THE routine inspection of steam generator tubing of pressurized water reactors of nuclear power plants, the eddy-current testing (ECT) using sinusoidal mode was used extensively for the detection and shape characterization of defects. The fastness and reliability of the method are counterbalanced, due to skin effect, by its limitation to thin and nonmagnetic structures. For deeper structures, including magnetic materials, pulse ECT (PECT) emerged recently as a robust and effective solution. The rectangular pulse profile accounts for a multifrequency analysis, higher harmonics penetrating deeper inside the material. Moreover, by reducing the pulse duration, the total amount in the power can be increased accordingly without exposing the probe and the material to extensive heat [1]–[3]. Although more sensitive to liftoff errors [4], [5] than classical ECT method, PECT was proposed for various industrial applications [1]–[3], including detection of defects in multiple-layered structures around fasteners in aeronautics, crack detection in structural steels [2], and nondestructive inspection in ferromagnetic tubes [3]. Solution of the inverse problem consisting in the reconstruction of shape of defects requires repeated calculation of a large number of forward problems. Fast and precise solutions of eddy-current problems, using integral approach, were proposed in [6]–[8]. For the reconstruction of defects with zero thickness in conductive media, methods combining a fast-forward solution and inversion using genetic algorithms were proposed [9]. In this paper, we introduce the method to detect the presence and reconstruct the shape of zero-thickness cracks using simulated pulse eddy currents in nonlinear magnetic materials, based on a model-free, using neural network (NN) inversion procedure.

II. Nonlinear Integral Formulation for the Direct Problem

The proposed method is based on application of **T**-electric potential to the integral equation of eddy currents, like in [9]. Starting from Maxwell equations in quasi-stationary form and the constitutive relationships

$$\mathbf{E} = \rho \cdot \mathbf{J} \tag{1}$$

$$\mathbf{H} = F(\mathbf{B}) \tag{2}$$

where $\boldsymbol{J}$ is the current density, $\boldsymbol{E}$ is the electrical field, ρ is the resistivity in the conductive domain Ω_c, $\boldsymbol{H}$ is the intensity of the magnetic field in the ferromagnetic media Ω_F, and $\boldsymbol{B}$ is the magnetic flux density in the whole domain $\Omega = \Omega_c \cup \Omega_0$. In the laboratory frame, the electrical field is

$$\mathbf{E} = -\frac{\partial \mathbf{A}}{\partial t} - \nabla V \tag{3}$$

where V is the electric scalar potential and $\mathbf{A}$ is the magnetic vector potential. The magnetic vector potential can be calculated using Biot–Savart formula

$$\mathbf{A} = \frac{\mu_0}{4\pi} \int_{\Omega} \frac{\mathbf{J}}{r} d\upsilon + \frac{\mu_0}{4\pi} \int_{\Omega} \frac{\nabla \times \mathbf{M}}{r} d\upsilon + \mathbf{A}_0 \tag{4}$$

where $\mathbf{A}_0$ is the magnetic vector potential due to the impressed current sources

$$\mathbf{A}_0 = \frac{\mu_0}{4\pi} \int_{\Omega_0} \frac{\mathbf{J}_0}{r} dV \tag{5}$$

and Ω_0 is the air. Only conductive and nonlinear media are meshed. The current density is expressed in terms of shape functions associated to the edges in the inner cotree [9]

$$\mathbf{J} = \sum_{k=1}^{n} \mathbf{N}_k \nabla \times \mathbf{T}_k \tag{6}$$

while the magnetization $\mathbf{M}$ is approximated as a piecewise uniform field

$$\mathbf{M} = \sum_{k=1}^{n} \mathbf{N}_k \mathbf{P}_k. \tag{7}$$

Applying Galerkin approach, the following equation system is obtained:

$$[R][I] + [L]\frac{d[I]}{dt} = [U] + [V] \tag{8}$$

Manuscript received June 28, 2013; revised August 5, 2013; accepted September 18, 2013. Date of current version February 21, 2014. Corresponding author: G. Preda (e-mail: gabriel.preda@upb.ro).
Digital Object Identifier 10.1109/TMAG.2013.2283194

where the terms of matrices [$\boldsymbol{R}$] and [$\mathbf{L}$] are calculated as

$$R_{ij} = \int_{\Omega_c} \nabla \times \mathbf{T}_i \cdot \rho \nabla \times \mathbf{T}_j \mathrm{d}v_c \tag{9}$$

and

$$L_{ij} = \frac{\mu_0}{4\pi} \int_{\Omega_c} \int_{\Omega_c} \frac{\nabla \times \mathbf{T}_i \cdot \nabla \times \mathbf{T}_j}{r} \mathrm{d}v_c \mathrm{d}v_c \tag{10}$$

and the right-hand side term U_i, due to impressed currents is calculated as

$$U_i = -\frac{\partial}{\partial t} \left(\frac{\mu_0}{4\pi} \int_{\Omega_c} \int_{\Omega_0} \frac{\nabla \times \mathbf{T}_i \cdot \mathbf{J}_0}{r} \mathrm{d}v_c \mathrm{d}v_0 \right) \tag{11}$$

with Ω_0 being the domain of impressed currents and $\mathbf{J}_0$ being the current density inside Ω_0. U_i results from $\mathbf{A}_0$ component of A, projected on the shape functions, and integrated over the whole conductive domain Ω_c.

The term V_i due to magnetization is calculated as

$$V_i = -\frac{\partial}{\partial t} \left(\frac{\mu_0}{4\pi} \int_{\Omega_c} \nabla \times \mathbf{T}_i \int_{\Omega_F} \frac{\mathbf{M} \times \mathbf{r}}{r^3} \mathrm{d}v_c \mathrm{d}v_F \right) \tag{12}$$

with Ω_F being the ferromagnetic domain. With $\mathbf{M}$ approximated constant in each subdomain of the finite-element discretization of the ferromagnetic media, (12) can be rewritten as

$$V_i = \frac{\partial}{\partial t} \sum_{k=1}^{n_F} \mathbf{a}_{ik} \cdot \mathbf{M}_k \tag{13}$$

where

$$\mathbf{a}_{ik} = \frac{\mu_0}{4\pi} \left(\int_{\Omega_c} \nabla \times \mathbf{T}_i \times \int_{\omega_{F(k)}} \frac{\mathbf{r}}{r^3} \mathrm{d}v_c \mathrm{d}v_F \right). \tag{14}$$

In (14), $\omega_{F(k)}$ is one of the subdomains used for the discretization of the ferromagnetic media. The nonlinearity is considered by the polarization term $\boldsymbol{I}$ [10]

$$\mathrm{I} = \mathbf{B} - \mu F(\mathbf{B}) \equiv G(\mathbf{B}). \tag{15}$$

The polarization fixed point method consists in the following iterative process:

1) a value for $\boldsymbol{I}^{(0)}$ is chosen;
2) at each step n, $n > 1$, $\boldsymbol{B}$ and $\boldsymbol{H}$ are computed from linear equations and therefore

$$\mathbf{B}^n = L\left(\mathbf{I}^{n-1}\right) \tag{16}$$

where L is a linear function;
3) the new polarization is obtained from (15)

$$\mathrm{I}^n = G\left(\mathbf{B}^n\right). \tag{17}$$

The above scheme is a Picard–Banach procedure for computing the fixed point of the function $\boldsymbol{W} = \boldsymbol{GL}$. We choose a working $\mu = \mu_0$ and we obtain

$$\left\| \mathbf{W}(\mathbf{I}^n) - \mathbf{W}(\mathbf{I}^{n-1}) \right\| \leq \eta \left\| \mathbf{I}^n - \mathbf{I}^{n-1} \right\|. \tag{18}$$

To increase the convergence speed, an over-relaxation technique is proposed to obtain an improved $\boldsymbol{I}^{(\mathrm{n})}$

$$\overset{\frown}{\mathbf{I}}^{(n)} = \mathbf{I}^{(n-1)} + \omega\left(\mathbf{I}^{(n)} - \mathbf{I}^{(n-1)}\right). \tag{19}$$

Time step and mesh size are adapted for each problem configuration, to account the fast variable regime of pulse eddy currents and for the equivalent small skin depth corresponding to pulse higher harmonics components [9]. Solution of one forward problem uses Crank–Nicholson with $\Theta = 1/2$ for time variation and polarization method with over-relaxation for nonlinear iterations [10]. Lower-Upper (LU) decomposition is used for the solution of linear system resulted for each nonlinear iterations, time, and scan steps.

III. Inverse Problem Solutions Using NNs

Defect shape reconstruction consists in the solution of an inverse problem: from the signals of magnetic flux density (inputs), we obtain the parameters for defects geometry (output values). An NN approach based on a highly customizable open source solution [11] is used. A database of signal–defect parameters (input–output) data is generated from successive simulations of forward problems [12], [13]. Then, the data are divided in training and validation (test) sets. Training data are used for the training of the NN. Each training epoch, node weights are recalculated and the error of the training is evaluated. Training will end after a predefined number of epochs or when a preset error threshold is reached. Periodically, at a given interval of training epochs, we propagate through the NN the testing data sets, to validate independently the error of reconstruction. If the randomly generated defect parameter data are covering uniformly the problem space, test error will show a similar evolution with the training error. After training ends, we will retain the best NN weights configuration, corresponding to the training epoch with the best results in terms of validation error.

A set of fresh signal (input) data is presented to the NN for verification. The resulted output data represent the reconstructed defect geometry corresponding to the fresh signal data presented to the NN.

IV. Numerical Results

Here, we show results for the reconstruction of outer, zero-thickness defects in a plate made of ferromagnetic material excited with a pancake shaped coil and a Hall sensor to pick up the signal. The pancake coil Hall sensor system is less sensitive to frequency variation and liftoff error than the autoinduction pancake coil used in AC ECT [1], [5], and [9]. The plate is 16 cm × 16 cm, with width 10 mm, the exciting coil dimensions are inner radius $R_{\min} = 2$ mm, outer radius $R_{\max} = 5$ mm, axial length $l_z = 4$ mm, and liftoff $z = 0.4$ mm. The pickup sensor measures the z-component of magnetic flux density and is placed in the z-axis of the exciting coil, at $z = 0.4$ mm. The coil signal is a 70 μs (with 10 μs rise and fall), trapezoidal shaped pulse, with an amplitude of $I_{\max} = 1000$ AT and a repetition frequency of 25 Hz. Scan path is 20 mm along a maximum 15 mm length defect zone, with the scan pitch of 2.5 mm.

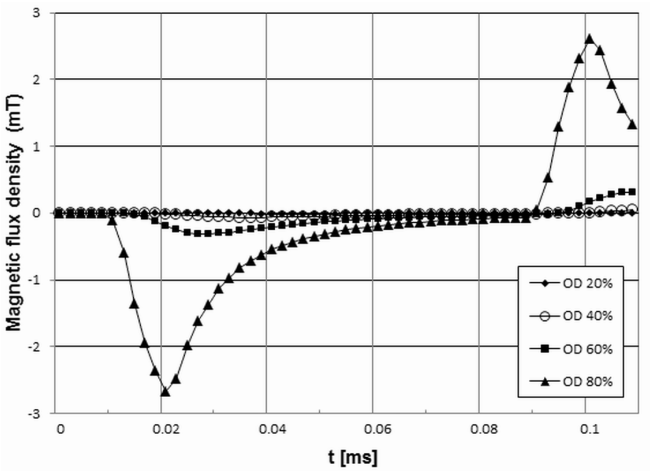

Fig. 1. Pickup signal for a 10 mm long defect. The signal is the difference between magnetic flux density measured in the case with crack and the case without crack. Defects are on the opposite side of the plate from the probe-pickup sensor system. Defects are 20%, 40%, 60%, and 80% from the plate thickness.

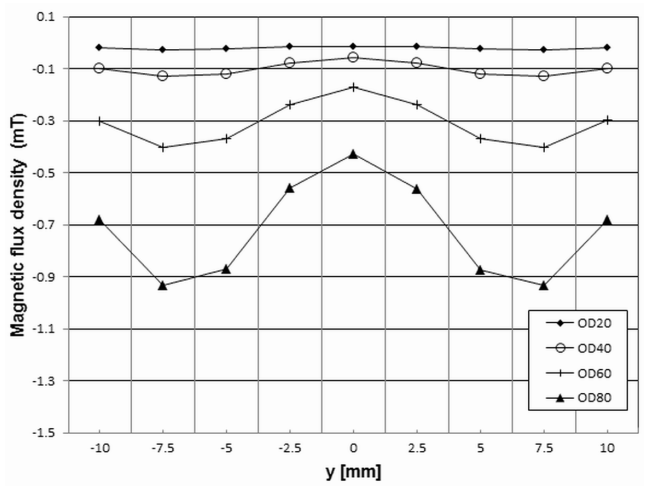

Fig. 2. Pickup signal for a 10 mm long defect (difference between magnetic flux density signal with crack and without crack). Scan path along the y-axis, parallel with the crack, 20 mm long. Defect, centered along the scan path, is on the opposite side of the plate from the probe-pickup sensor system. Defects are 20%, 40%, 60%, and 80% from the plate thickness.

In Fig. 1, we show the difference signal for a 10 mm long defect. Cracks have the opening in the opposite side of the plate [outer defects (ODs)], with depth from 20% to 80% from the plate thickness. We notice that the maximum of difference signal is reached at different time for different defect depths. The maximum value is reached for the 80% at $t = 21$ μs, and at $t = 44$ μs for the 20% depth OD.

Fig. 2 shows the signals picked up at the time moment $t = 44$ μs, along the scan path, for the same 10 mm longitudinal crack, for defects with depth from 20% to 80% from the plate thickness. The pickup time is selected to emphasize the effect of the deepest buried defects under plate surface.

In Fig. 3, we show the difference signal for a defect with 80% depth with various lengths, from 5 to 20 mm.

The accidental liftoff variation of the exciting coil-pickup sensor system can be a major perturbation for the measured signal [4], [5]. Fig. 4 shows the variation of the difference signal with the liftoff, for values of liftoff of 0.4, 0.6, 0.8,

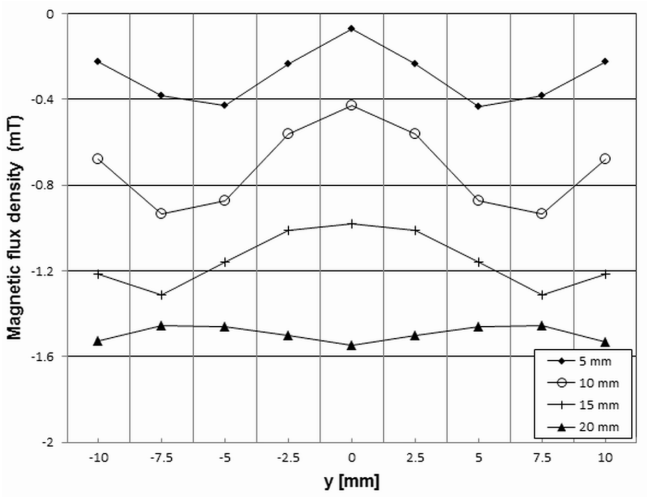

Fig. 3. Pickup difference signal for a defect with length of 5, 10, 15, and 20 mm. Scan path is along the y-axis, parallel with the crack. Signal picked up at $t = 44$ μs.

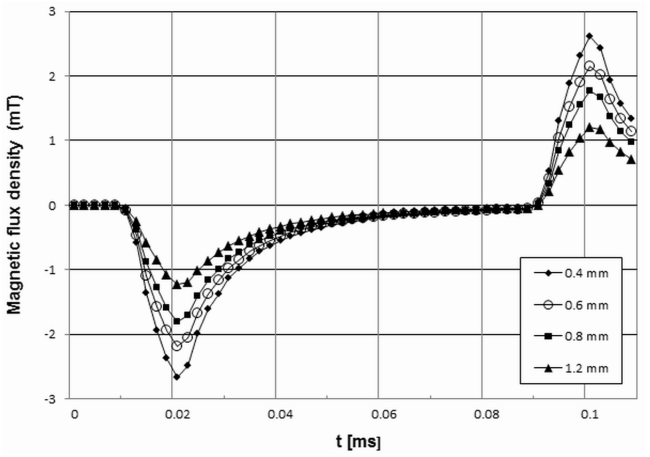

Fig. 4. Pickup signal in the point $y = 0$, along the scan path, for an 80% OD, 10 mm long, liftoffs of 0.4, 0.6, 0.8, and 1.2 mm.

and 1.2 mm, for an 80% OD, 10 mm long. For the training data used in the defect shape reconstruction, we only used simulated signals in the setup with liftoff of 0.4 mm, signals being sampled at $t = 44$ μs.

For each simulation, we compute the difference signal between the case with and without defect. The couple of difference signal and defect geometry parameters is used as an input–output pair in the training of an NN used for flaws shape reconstruction.

Defect parameterization method is shown in Fig. 5. Along the scan path, the plate discretization is uniform, with a constant mesh division in the scan direction and the plate thickness, respectively. For the simulations used in the training data, 2.5 mm long mesh division along the scan path and 1 mm in the plate thickness were used. Therefore, the defect zone is represented by a 10×10 cell matrix, or a 25 mm $\times$ 10 mm in y and z directions, respectively. Only a 15 mm area, along y-axis, is retained for defect parameterization, or six columns from the total of 10 columns. In each of these columns, defect depth, measured from the opposite side of the plate, can have from 0% to 90% of plate thickness.

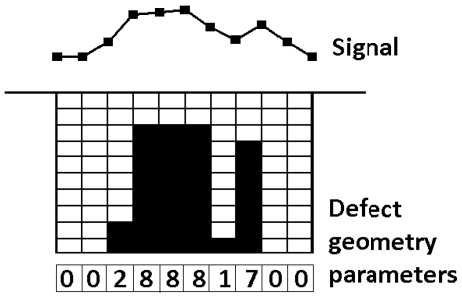

Fig. 5. Defect is parameterized using the depth of the defect along the scan area; in the example shown here, the defect parameters 0, 0, 2, 8, 8, 1, 7, 0, and 0 stand for 0%, 0%, 20%, 80%, 80%, 10%, 70%, 0%, and 0% depth of simulated defect along the scan line.

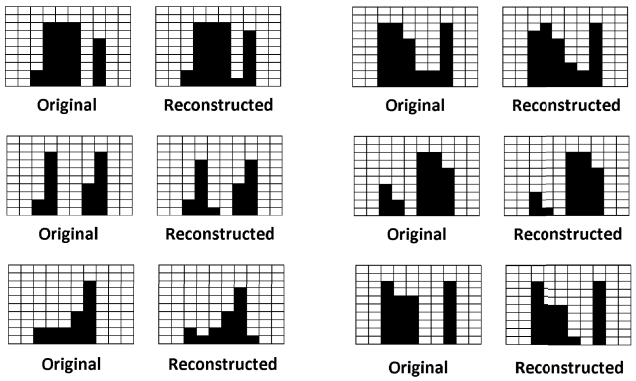

Fig. 6. Original and reconstructed defect geometries for six cases, selected from the total set of 10 verification data. Average mean square error for the verification data was 0.0028. Reconstructions using best NN configuration, with mean square error for training data 0.0028 and for test data 0.0035, achieved after 19 500 training steps.

A total of 700 defect configurations were simulated. From the total 700 resulted signal–defect geometry parameters pairs, 650 couples were presented to NN module for training, 40 were used for validation (test) and 10 were reserved for verification. Simulation for only one case, on a PC with Intel i7 CPU, eight cores, with 8 GB RAM and 3.2 GHz CPU speed, will take 1039 s, 2/3 of this time being used for calculation of double-volume integral matrices described by (10) and (14). For the full signal–defect pair database calculation, these expensive computations are done only once, since for all problems, geometry is not changing. Different defect configurations change only the cotree structure and not the volume elements [9]. Average duration for one nonlinear forward problem is for a full scan problem, 329 s, with 119 s the factorization time.

Best results were achieved with an NN setup implementing the improved resilient backpropagation algorithm, with sigmoid symmetric activation functions for both inner and outputs nodes. The number of input and output nodes is the same with the number of scanning points and defect parameters, i.e., 11 and six, respectively. The number of hidden nodes was selected to be 61, in a single layer. The NN training was stopped after 25 000 iterations, with training mean square error calculated 0.0032 and worst test error 0.004, while average test error was 0.003. Best training and test errors were achieved after 19 500 epochs, with training error 0.0028 and test error 0.0035, respectively, and the NN configuration for this epoch was used for propagation of the new data presented to the NN for reconstruction. Training and fresh data propagation total time took 86.2 s on the same PC used in forward problem simulation. In Fig. 6, we show six representative results for the fresh (verification) data; mean square error for all verification data was 0.0028.

V. Conclusion

Using pulse eddy currents for energizing the specimen and magnetic flux density as pickup signal allows us to emphasize the presence of defect buried deep under material surface. Deeper, smaller ODs produce difference signals with delayed peak values than closer-to-surface defects thus providing a better defect selectivity. Zero-thickness defects can be simulated with high accuracy using integral-FEM method. Since geometry is not changing, the most expensive computational effort is required only once for all successive simulations required for building the training database. The NN-based inversion technique provides an accurate and fast reconstruction of defect geometries.

References

[1] B. Lebrun, Y. Jayet, and J.-C. Baboux, "Pulsed eddy-current signal analysis: Application to the experimental detection and characterization of deep flaw in highly conductive materials," *NDT&E Int.*, vol. 30, no. 3, pp. 163–170, 1997.

[2] S. Xie, Z. Chen, T. Takagi, and T. Uchimoto, "Efficient numerical solver for simulation of pulsed eddy-current testing signals," *IEEE Trans. Magn.*, vol. 47, no. 11, pp. 4582–4591, Nov. 2011.

[3] B. Yang and X. Li, "Pulsed remote eddy current field array technique for nondestructive inspection of ferromagnetic tube," *Nondestruct. Test. Eval.*, vol. 25, no. 1, pp. 3–12, 2010.

[4] Y. He, M. Pan, and G. Tian, "Reduction of lift-off effects in pulsed eddy current for defect classification," *IEEE Trans. Magn.*, vol. 47, no. 12, pp. 4753–4760, Dec. 2011.

[5] G. Y. Tian, Y. Li, and C. Mandache, "Study of lift-off invariance for pulsed eddy-current signals," *IEEE Trans. Magn.*, vol. 45, no. 1, pp. 184–191, Jan. 2009.

[6] G. Rubinacci, A. Tamburrino, S. Ventre, and F. Villone, "A fast algorithm for solving 3-D eddy current problems with integral formulation," *IEEE Trans. Magn.*, vol. 37, no. 5, pp. 3099–3103, Sep. 2001.

[7] M. Morozov, G. Rubinacci, A. Tamburrino, and S. Ventre, "Numerical models of volumetric insulating cracks in eddy-current testing with experimental validation," *IEEE Trans. Magn.*, vol. 42, no. 5, pp. 1568–1576, May 2006.

[8] R. Albanese, G. Rubinacci, and F. Villone, "An integral computational model for crack simulation and detection via eddy currents," *J. Comput. Phys.*, vol. 152, no. 2, pp. 736–755, 1999.

[9] G. Preda, M. Rebican, and F. I. Hantila, "Integral formulation and genetic algorithms for defects geometry reconstruction using pulse eddy currents," *IEEE Trans. Magn.*, vol. 46, no. 8, pp. 3433–3436, Aug. 2010.

[10] F.I. Hantila, G. Preda, and M. Vasiliu, "Polarization method for static fields," *IEEE Trans. Magn.*, vol. 36, no. 4, pp. 672–675, Jul. 2000.

[11] S. Nissen. (2013, Mar. 5). *Fast Artificial Neural Networks Library* [Online]. Available: http://leenissen.dk/fann/wp/

[12] G. Preda, B. Cranganu-Cretu, F. I. Hantila, O. Mihalache, and K. Miya, "Nonlinear FEM-BEM formulation and model-free inversion procedure for reconstruction of cracks using eddy currents," *IEEE Trans. Magn.*, vol. 38, no. 2, pp. 1241–1244, Mar. 2002.

[13] R. C. Popa and K. Miya, "Approximate inverse mapping in ECT, based on aperture shifting and neural network regression," *J. Nondestruct. Eval.*, vol. 17, no. 4, pp. 209–221, 1998.